Cell. Mol. Life Sci. (2014) 71:2517–2533
DOI 10.1007/s00018-013-1498-7

Cellular and Molecular Life Sciences

RESEARCH ARTICLE

Protease-activated-receptor-2 affects protease-activated-receptor-1-driven breast cancer

Mohammad Jaber · Miriam Maoz · Arun Kancharla · Daniel Agranovich · Tamar Peretz · Sorina Grisaru-Granovsky · Beatrice Uziely · Rachel Bar-Shavit

Received: 6 February 2013 / Revised: 29 September 2013 / Accepted: 14 October 2013 / Published online: 1 November 2013
© Springer Basel 2013

Abstract Mammalian protease-activated-receptor-1 and -2 (PAR_1 and PAR_2) are activated by proteases found in the flexible microenvironment of a tumor and play a central role in breast cancer. We propose in the present study that PAR_1 and PAR_2 act together as a functional unit during malignant and physiological invasion processes. This notion is supported by assessing pro-tumor functions in the presence of short hairpin; *sh*RNA knocked-down *hPar2* or by the use of a truncated PAR_2 devoid of the entire cytoplasmic tail. Silencing of *hPar2* by *sh*RNA-attenuated thrombin induced PAR_1 signaling as recapitulated by inhibiting the assembly of Etk/Bmx or Akt onto PAR_1-C-tail, by thrombin-instigated colony formation and invasion. Strikingly, *sh*RNA-*hPar2* also inhibited the TFLLRN selective PAR_1 pro-tumor functions. In addition, while evaluating the physiological invasion process of placenta extravillous trophoblast (EVT) organ culture, we observed inhibition of both thrombin or the selective PAR_1 ligand; TFLLRNPNDK induced EVT invasion by *sh*RNA-*hPar2* but not by scrambled *sh*RNA-*hPar2*. In parallel, when a truncated PAR_2 was utilized in a xenograft mouse model, it inhibited PAR_1–PAR_2-driven tumor growth in vivo. Similarly, it also attenuated the interaction of Etk/Bmx with the PAR_1-C-tail in vitro and decreased markedly selective PAR_1-induced Matrigel invasion. Confocal images demonstrated co-localization of PAR_1 and PAR_2 in HEK293T cells over-expressing YFP-*hPar2* and HA-*hPar1*. Co-immuno-precipitation analyses revealed PAR_1-PAR_2 complex formation but no PAR_1-CXCR4 complex was formed. Taken together, our observations show that PAR_1 and PAR_2 act as a functional unit in tumor development and placenta-uterus interactions. This conclusion may have significant consequences on future breast cancer therapeutic modalities and improved late pregnancy outcome.

Keywords PAR_1 PAR_2 · Protease · GPCR · Thrombin · Breast tumor

Introduction

G protein-coupled receptors (GPCRs) represent the largest family of cell surface receptors [1, 2] and are divided into six subfamilies (classes A–F) based on their ligand interaction and signature residues [3, 4]. Many class A subfamily are major drug targets [5] among which are mammalian protease-activated receptors (PARs). There are four PAR family members (PAR1–4), all of which are proteolytically activated at the N-terminal extra-cellular domain generating a new N-terminal site that functions as a tethered ligand by binding intramolecularly to the second loop of a given PAR [6]. Class A receptors are characterized by several features among which are conserved motifs in the third trans-membrane domain (TM3), three cytoplasmic loops (C1, C2, and C3), and a C-terminal tail (C4). X-ray structure of rhodopsin, a prototype of class A receptor, revealed the presence of a highly conserved amphipathic 8th helix

Electronic supplementary material The online version of this article (doi:10.1007/s00018-013-1498-7) contains supplementary material, which is available to authorized users.

M. Jaber · M. Maoz · A. Kancharla · D. Agranovich · T. Peretz · B. Uziely · R. Bar-Shavit (✉)
Sharett-Institute of Oncology, Hadassah-Hebrew University Medical Center, POB 12000, 91120 Jerusalem, Israel
e-mail: Rachelbar@ekmd.huji.ac.il

S. Grisaru-Granovsky
Department of Obstetrics and Gynecology, Shaare-Zedek and Hadassah-Hebrew University Medical Centers, POB 12000, 91120 Jerusalem, Israel

(H8) within the C-tail that is likely to be physically interposed between the receptor and G protein [7]. Indeed, the H8 helix loop was also described in other class A receptors including PAR_1 and PAR_2 [8] and is formed by anchoring to the membrane by palmitoylation of the C-terminal cysteine residues.

Our view regarding the regulation and signaling of the large GPCR family has greatly evolved over the last several years. It has become apparent that while GPCRs switch between active conformations (capable of activating G proteins), and inactive conformations (that do not activate G-proteins) [9, 10]; additional options of activation exist. Adding to the complexity of GPCR signaling, it is now clear that GPCRs are capable of adopting more than one active conformation, in which each active state is capable of stimulating an overlapping yet distinct group of downstream effectors [9]. These properties are recapitulated by the discovery of biased-agonism/antagonism or as more frequently referred "biased-ligands". This term has become synonymous with additional terms to indicate the more likely selective activation of GPCR signaling pathway for functional selectivity and including stimulus trafficking [11]. It allows an agonist to bind preferentially and stabilize one active signaling state over another, thus endowing the term activation in a more profound meaning, illustrating in-depth the dynamic nature of GPCR-stabilized signal activation.

Overall, the elucidation in recent years of the crystal structures of several archetypal GPCRs, such as rhodopsin [7], chemokine receptors, as well as others (such as: β_2 and β_1-adrenergic receptors; [12, 13], A_{2A} adenosine receptor; [14, 15], dopamine D3 receptor; [16], and chemokine CXCR4 receptor; [17]) has provided new insights into the common features of general structures. It has become more evident that the significant differences and selectivity of receptors in fact relies on the extracellular/transmembrane ligand binding site determining a receptor with its unique features. In addition, the technology of high-resolution crystal structure of class A GPCRs demonstrated homodimer formation (as seen by the opioid receptors [18] and by CXCR4 [19]) and heterodimers. Evidence is accumulating showing that chemokine receptors, for example, can dimerize [19, 20]. CCR2 and CXCR4, which are more distantly related, form heterodimers as revealed by the observation that specific antagonists of one receptor inhibit the binding of chemokines to the other receptor [21]. The current emerging prospect is that dimers or oligomers of GPCRs are the functional units that interact with heterotrimeric G proteins and arrestins for signal generation and receptor desensitization. This form of heterodimer generation adds another layer of complexity to the regulation of GPCR signaling. GPCR heterodimerization affects receptor conformation and contributes to the activation of selective signaling, adding an extra level to the multifaceted action of GPCRs.

Members of the mammalian PAR family have been shown to form heterodimers. PAR_1/PAR_3 heterodimerization is required in endothelial cells for regulation of cell permeability in response to thrombin [22]. PAR_1 and PAR_4 also form stable heterodimeric complexes on the surface of platelets and PAR_1 appears to assist in the activation of PAR_4 in platelet-mediated thrombosis [23]. Recent studies suggest that PAR_1 and PAR_2, relatively distant receptors, exist in close proximity on the cell surface and can signal together during acute vascular inflammation [24]. The molecular basis for this interaction has been elucidated in endothelial cells, fibroblasts, and human embryonic kidney cells, whereby thrombin-cleaved PAR_1 donates its tethered ligand to transactivate PAR_2 [25, 26]. Although PAR_2 is not activated directly by thrombin, the thrombin-generated PAR_1-tethered ligand, SFLLRN, serves as an agonist for PAR_2 [26, 27]. Sevigny et al. [28] have demonstrated that knocking-out PAR_2 expression reduced neointimal vasculature hyperplasia induced by PAR_1. Recently, it was demonstrated that PAR_1 drives the trafficking behavior of PAR_2, but not vice versa. Furthermore, thrombin activation of PAR_1–PAR_2 heterodimer results in co-internalization and β-arrestin recruitment, an event that is not observed with the activated PAR_1 alone. Therefore, a biased and specific signaling response is demonstrated by PAR_1–PAR_2 inducing a distinct signaling β-arrestin recruitment [29].

Here, we demonstrate that PAR_1-induced tumor-promoting processes depend on the presence of a PAR_2. This was shown by either *sh*RNA silencing of PAR_2 expression or by the use of a truncated PAR_2 construct. The importance of the PAR_2 C-tail was evaluated in co-IP assays between PAR_1 and signal proteins, colony formation in soft agar, migration and invasion, in vitro as well as tumor growth in a xenograft mouse model in vivo. Co-localization of PAR_1–PAR_2 was established by confocal immunofluorescence and co-IP between PAR_1 and PAR_2 but not CXCR4. It is well recognized in a physiological invasion process that placenta trophoblasts anchor to the uterus deciduas, in a similar manner as tumor cell invasion, providing an attractive model to study a highly regulated invasion scheme [30–32]. We demonstrate that *sh*RNA-*hPar2* silencing significantly inhibits thrombin-activated extravillous trophoblast (EVT) invasion in an organ culture system, recapitulating cytotrophoblast invasion in vivo. This was shown in the first-trimester trophoblasts that act in the establishment and bridging into the maternal tissues. Hence, PAR_2 is also required for EVT invasion. Altogether, silencing of *hPar2* expression or the use of a truncated PAR_2 form modulates PAR_1-induced tumor function. Our findings can be partially explained by the

formation of PAR_1–PAR_2 functional unit, in PAR-driven breast tumor.

Experimental procedures

Cells

Breast cancer cells; MCF7, MDA-MB-231, and MDA-MB-468 (ATCC VA, USA) and HEK293T cells were maintained in DMEM with 10 % fetal calf serum. HU breast epithelial cells were generated by the late Dr. Aviva Horowitz of the Sharett-Institute of Oncology, Hadassah-Hebrew University Medical Center, Jerusalem.

Plasmids and transfection

A cDNA encoding wild-type human *Par2* was kindly provided by Prof. Morley D. Hollenberg (Faculty of Medicine, University of Calgary, Canada). Truncated *hPar2* were generated by insertion of a stop codon at position *K348Z* of *hPar2*. This was prepared by using QuikChange Lightning Site-Directed Mutagenesis Kit (Agilent Technologies Stratagene, Santa Clara, CA, USA) according to the manufacturer's instructions. The designated primer used for inserting the stop codon TCA in *hPar2* at position K348 is *S348Z*-5′-CGACCCCTTTGTCTAT TACTTTGTT**TCA-**CATGATTTCAGGG-3′. MCF7 (of endogenous *hPar2*) or HU (do not express either *hPar1* or *hPar2*) cells were transfected with 1–2 μg of cDNA encoding wt human *hPar1* or HA-tag-*hPar1* or *hPar2* or truncated *hPar2* (devoid of the cytoplasmic tail), or T7-tag-*etk/bmx* or with a control pcDNA3 vector (Invitrogen, Carlsbad, CA, USA) using FuGene transfection reagent (Roche Molecular Biochemicals, Indianapolis, IN, USA). Transfected cells were selected with G418 (800 μg/ml) to obtain stable populations of cells expressing *hPar1* and *hPar2* or *hPar1* and truncated *hPar2*.

RNA isolation and RT-PCR

RNA was isolated with Tri-Reagent (MRC, Cincinnati, OH, USA) according to the manufacturer's instructions. After reverse transcription of 1 μg total RNA by oligo (dT) priming, cDNA was amplified using Taq DNA polymerase (Promega, Madison, WI, USA). Comparative semi-quantitative PCR was performed using the following primers: GAPDH sense: 5′-CCACCCATGGCAAATTCCATGGC-3′ and antisense: 5′-TCTAGACGGCAGGTCAGGTCC ACC-3′ primers. PAR_1 N-terminus primers were as follows: *hPar1*-sense: 5′- CTCGTCCTCAAG GAGCAAAC-3′, antisense orientation: 5′-TGGGATCGGAACTTTCTTTG-3′ (resulting with a 564-bp PCR product). PAR_2 primers: F: 5′-GGCCAATCTGGCCTTGGCTGA C-3′; R: 5′-GGC AGGAATGAAGATGGTCTG-3′.

Generation of *sh*RNA for *hPar2*

To prepare *sh*RNA constructs, we used a U6 promoter—driven and lentivirus (pLentiLox 3.7)—mediated delivery cassette of *sh*RNA containing a stem-and-loop structure based on a 19-nucleotide sequence from the *hPar2* coding region. shRNA cassette sequences were then ligated into pLentiLox 3.7 vector that encodes GFP (gift of Van Parij Laboratory, Massachusetts Institute of Technology, Cambridge, MA, USA). The sequence of shRNA for the *hPar2* target gene is 5′- GGAAGAAGCCTTATTGGTA-3′. Scrambled *sh*-RNA *hPar2* is 5′-GCAA GGTA AGCG-TATGTTA-3′. The lentivirus particles were generated by a three-plasmid expression system, in which 293T cells were co-transfected with the following three vectors: packaging (CMVD R8.91), envelope (CMV-VSV-G), and the transfer vector pLentiLox 3.7. 293T cells were plated to 60 % confluency 1 day before transfection. Cells were transfected in fresh medium the following day with the three plasmids using Fugene 6 transfection reagent. Medium was replaced with fresh medium 24 h later. On days 2 and 3 after transfection, medium was collected and the viral particles were concentrated 100-fold by centrifuging for 1 h at 40,000 rpm.

Generation of a mutant R36A PAR_2. In the extra-cellular portion of PAR_2

GR/SLIGK whereby R36 was changed to A to generate R36A mutant by using QuikChange site-directed mutagenesis (Agilent Technologies, Santa Clara, CA, USA) using the following primer: 5′-GA ACC AAT AGA TCC TCT AAA GGA **GCA** AGC CTT ATT GGT AAG GTT GAT-3′. The inserted mutant R36A was confirmed by didoxy sequencing.

Western-blot and immunoprecipitation analysis

Cells were activated with agonist peptide TFLLRNPNDK for the indicated periods of time and solubilized in lysis buffer containing10 mM Tris–HCl, pH 7.4, 150 mM NaCl, 1 mM EDTA, 1 % TritonX-100, and protease inhibitors (5 mg/ml aprotinin, 1 mM phenylmethylsulfonylfluoride, and 10 mg/ml leupeptin) at 4 °C for 30 min. The cell lysates were subjected to centrifugation at 12,000 rpm at 4 °C for 20 min. Supernatant (400 μg) was incubated with on of the following antibodies: anti-PAR_1 (ATAP, Santa Cruz, CA, USA; 1 μg/ml), anti-HA (HA.11 mAb COVANCE, Berkeley, CA, USA), anti-PAR_2 (SAM11; Santa Cruz, CA, USA; 5 μg/ml), anti-GFP (mAb 6556; Abcam,

Cambridge, England) or anti-T7 (T7-Tag antibody; Novagen, Madison, WI, USA). After overnight incubation, protein A-sepharose beads (Amersham Pharmacia Biotech, Buckinghamshire, UK) were added to the suspension (50 µl), which was rotated at 4 °C for 1 h. Extensive washes with lysis buffer then followed to specifically obtain the immunocomplexes. The immunocomplexes were eluted and separated on a 10 % SDS-PAGE gel, followed by transfer to an Immobilon-P membrane (Millipore, USA). Membranes were blocked and probed with 1 µg/ml amounts of the appropriate antibodies as follows: anti-PAR_1 thrombin receptor mAb, (ATAP, from Santa Cruz, 1:1,000); anti-T7 (T7-Tag antibody; Novagen, Madison, WI, USA, 1:1,000) or a polyclonal anti-phospho-Akt (ser 473; 1:1,000; Cell Signaling, Boston, MA, USA), suspended in 3 % BSA in 20 mM Tris–HCl, pH 7.5, 15 mM NaCl, and 0.1 % Tween-20. After washing, the blots were incubated with secondary antibodies conjugated to horseradish-peroxidase. Immunoreactive bands were detected by enhanced chemiluminescence (ECL). Membranes were stripped and incubated with anti-IP antibodies to ensure equal protein load.

PAR_1 and PAR_2 and PAR_4 activation and antagonist

Thrombin as an activator was used at 1 U/ml (e.g., 10 nM). Selective PAR_1 activation was carried out by either TFLLRN or TFLLRNPNDK peptide and PAR_2 activation by SLIGKV. PAR_1 antagonist; SCH79797 (sc-203693, Santa Cruz Biotechnology, Inc. Dallas, TX, USA). PAR_4 ligand; AYPGKF (GenSript, Piscataway, NJ, USA). tcY-NH_2; PAR4 antagonist (Tocris Bioscience Inc, Minneapolis, MN, USA).

Immunofluorescence

HEK293T cells were plated on cover-slips that were precoated with poly-L-lysine, at least 24 h prior to transfections. Cells were transfected either with YFP-*hPar2* (kindly provided by Dr. Morely D. Hollenberg, Department of Pharmacology and Therapeutics and Medicine, University of Calgary, Calgary, Canada; 0.5 µg/ml) or HA-*hPar1* (0.5 µg/ml) or both for 48 h and then activated. Twenty-four hours before activation, the cells were starved in medium with 0.2 % BSA. The cells were activated by thrombin for brief periods (e.g., 2′, 5′ and 10 min) and then the medium was aspirated and the samples were washed twice with cold PBS and fixed with absolute cold methanol. Fixed cells were incubated with anti-HA antibodies (10 µg/ml, Covance Inc., Princeton, NJ, USA) followed by Cye3-conjugated anti-mouse IgG (4 µg/ml; Jackson Immuno-research Laboratories, PA, USA) as secondary antibodies. PAR_2 was detected directly by fluorescence imaging (green) of the YFP (at 514 wave length; 514–542). Nuclear staining was performed using DRAQ5 (4 µM; Cell Signaling; Boston, MA, USA). Images were obtained using a Zeiss LSM 5 confocal microscope and analyzed with Zen software (Carl Zeiss).

Colony formation in soft agar

A total of 5×10^3 cells per well were plated on a 0.5 % agarose base in six-well plates in growth medium containing 0.35 % agarose. Cells were either thrombin activated (1 U/ml) or not (control) added every 48 h. After 12 days of incubation, images of the colonies were either taken with phase microscopy or after staining with 0.005 % crystal violet at room temperature for 1 h.

Placenta tissue collection and preparation

Placental tissues were prepared as previously described [32]. Briefly, the placental tissues were extracted from discarded material provided by patients who voluntarily and legally chose to terminate pregnancy during the first trimester (between 5 and 12 weeks gestation). Gestational age was determined by the date of the last menstrual period and ultrasound measurement of the crown-rump length. All specimens were obtained strictly in adherence with the Hadassah Hospital Institutional Ethics Committee Guidelines.

First-trimester villous explants in cultures

The preparation and cultivation of villous explants of different first-trimester placentas were performed as described elsewhere [32–34]. Briefly, the placental tissue originated from samples between 7 and 9 weeks gestation were immediately rinsed in sterile cold phosphate-buffered saline (PBS) and processed within 2 h of collection. Following dissection under microscope, approximately 2–5 mg weight specimens were carefully laid on 200 µl of solid reconstituted undiluted Matrigel substrate (Becton–Dickinson, Bedford, MA, USA) in 0.4 µm pore-culture Millicell-CM culture dish inserts (pore size 0.4 µm, Millipore Corp., Bedford, MA, USA). Explants were cultured in DMEM/F-12 supplemented with 100 U/ml penicillin, 100 µg/ml streptomycin, and 0.25 µg/ml ascorbic acid, pH 7.4. Villous explants were maintained in culture for 3 days. Viability of the explants was assessed by adherence to Matrigel and emerging EVTs breaking from the tips as observed under a phase microscope. At 24 h in culture, explants were treated with thrombin (1 U/ml), TFLLRN (100 µM), and SLIGKV (100 µM) and infected or not with *sh*RNA *hPar2*- GFP- or scrambled *sh*RNA*hPar2* viral vector. After 72 h in culture, the Matrigel cast cylinders with

the EVTs were detached from the base of the insert cells by fine dissection under the microscope, fixed in 4 % paraformaldehyde, embedded in paraffin and further processed for histochemical tissue analysis. Each experimental condition was carried out in triplicate originating from eight different placental sets samples.

EVT invasion assessment

We assessed the H&E-stained serial sections of the EVT. We limited our study to the trophoblasts that penetrated through the Matrigel but remained on the surface of the polycarbonate membrane, that is, within the cast [33, 35, 36]. These were visualized on sequential slices of the entire Matrigel cast by hematoxylin staining. Slides were photographed by digital image capture software and all specimens were evaluated by two of the authors (S.G–G. and M.M.). Depth of invasion was assessed for each experiment (disappearance of trophoblast cells on the serial sections). At the deepest common level of invasion the total EVT cells at five randomly selected microscope fields (magnification 40×) were counted, for each experimental condition and the mean ± SEM/HPF calculated.

Matrigel invasion assay

Blind-well chemotaxis chambers with 13-μm-diameter filters were used for this assay. Polyvinylpyrrolidone-free polycarbonate filters, 8 μm pore size (Costar Scientific Co. Cambridge, MA, USA), were coated with basement membrane Matrigel (50 μl of 10 mg/ml Matrigel applied per blind well; 25 μg/filter). Briefly, the Matrigel was diluted to the desired final concentration with cold distilled water, applied to the filters and dried under a hood. Cells (2×10^5) suspended in DMEM were added to the upper chamber. Conditioned medium of NIH-3T3 fibroblasts was added to the lower compartment of the Boyden chamber as a chemoattractant. Assays were carried out at 37 °C in 5 % CO_2. Following incubation, cells on the upper surface of the filter were removed by wiping with a cotton swab. The filters were fixed and stained with DifQuick System (Dade Behring Inc, Newark, NY, USA). Cells from various areas of the lower surface were counted and each assay was performed in triplicate.

Animal studies

Female athymic nude mice at 6–8 weeks of age were implanted subcutaneously with 2×10^6 HU cells stably transfected with either *hPar1* and *hPar2, hPar2* alone, or *hPar1* and a truncated form of *hPar2*. Mice were monitored for tumor size by external caliber measurements (length and width) at the time points indicated. Tumor volume (V) was calculated by $V = L \times W^2 \times 0.5$, where L is length and W is width. After 3 weeks, the mice were killed and the tumors were excised, measured, and weighed ($n = 5$). All animal experiments were strictly in adherence with the Hadassah-Hospital Institutional Ethics Committee guidelines and approved by the animal committee of the Hebrew University, Jerusalem, Israel (MD-107.05-4).

Results

The silencing of *hPar2* inhibits the association of signaling partners on PAR_1 C-tail

Etk/Bmx specifically associates with the PAR_1-C-tail via its pleckstrin homology (PH) domain and forms a scaffold assembly site that initiates the cell-signaling network [37]. To examine whether the association between the PAR_1-C-tail and Etk/Bmx is modulated by PAR_2, we utilized MCF7 clones expressing either HA-*hPar1* and T7-tag-Etk/Bmx, HA-*hPar1* 7A mutant, which fails to bind Etk/Bmx (see supplementary data, Fig. S1A&B) or scrambled short hairpin (*sh*) RNA *hPar2* in the presence of HA-*hPar1* and T7-Etk/Bmx. Co-immuno precipitation analyses showed that while Etk/Bmx is immobilized onto PAR_1-C-tail following thrombin activation, this complex formation is completely abrogated when *hPar2* is knocked down (MCF7 cells express endogenously moderate levels of PAR_2) (Fig. 1Ai and Supplementary data S4C). The complex formation is observed in the presence of scrambled *sh*RNA-*hPar2,* similar to the association between control, non-treated cells of Etk/Bmx and PAR_1-C-tail in MCF7 clone over-expressing HA-*hPar1* and T7-tag-Etk/Bmx (Supplementary data Figs. S1 and S2). No co-immunoprecipitation was seen following empty vector transfection (data not shown). Strikingly, in the presence of *sh*RNA-*hPar2* inhibition of the specific TFLLRN PAR_1 ligand [38] induced Etk/Bmx-PAR_1 complex is observed as compared with the scrambled *sh*RNA-*hPar2* following TFLLRN activation (Fig. 1Aii). Interestingly, SLIGKV selective PAR_2 activation also results with the immobilization of Etk/Bmx onto PAR_2 C-tail (Kancharla A et al, Manuscript in preparation). Therefore, it appears that both PAR_1 and PAR_2 follow at least partly, a similar pattern of signal activation.

We also examined in these clones the interactions between the PAR_1-C-tail and Akt, a prime signaling partner in cancer cells. For this purpose, anti-HA antibodies were used to immunoprecipitate the HA-tagged PAR_1 protein, following thrombin activation. Association of Akt with the PAR_1 C-tail increased with time. Furthermore, using anti-phospho-Akt antibodies, it is demonstrated that PAR_1-bound Akt undergoes phosphorylation, indicating that Akt is functional in the PAR_1-immobilized state. Knocking

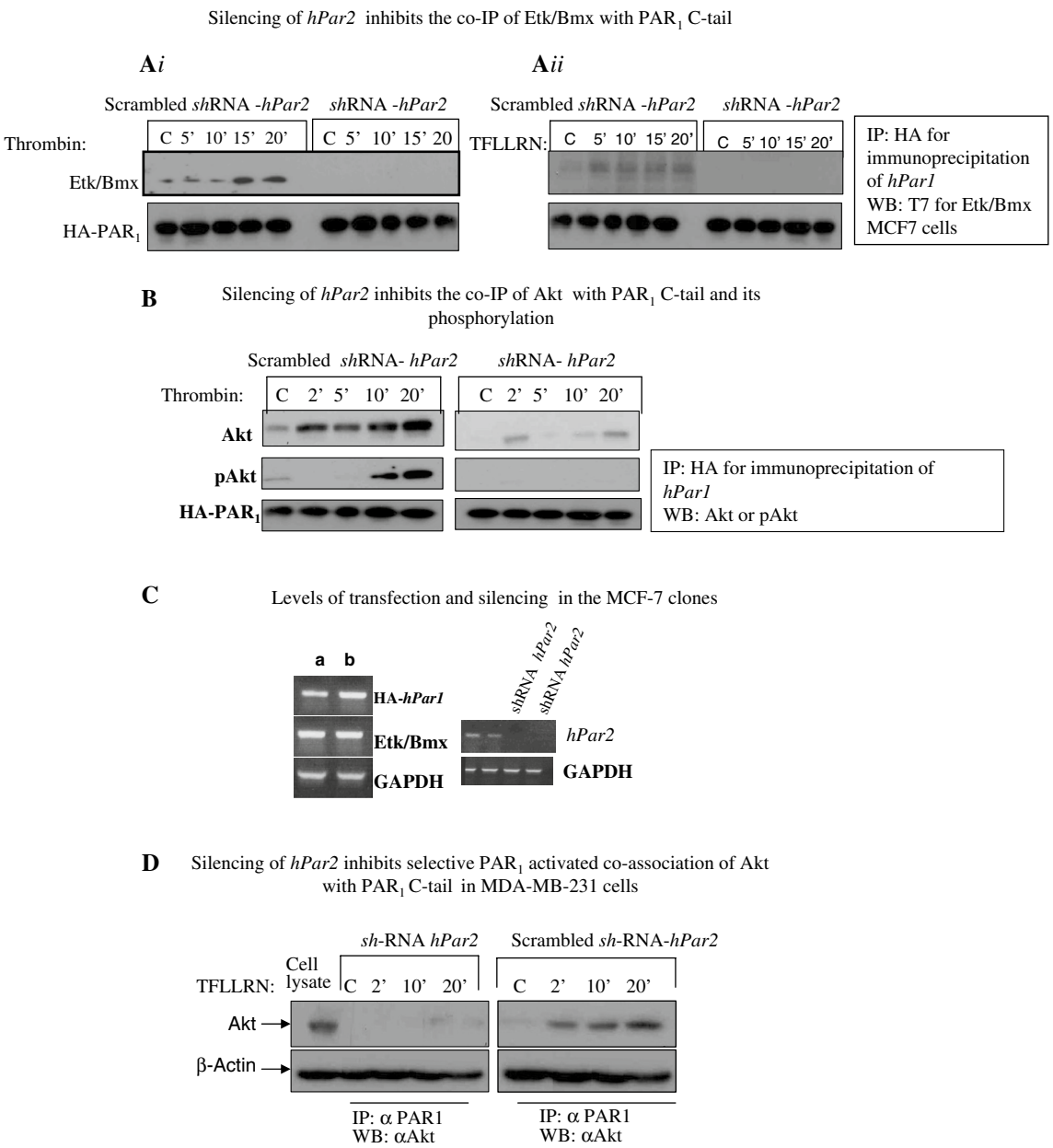

Fig. 1 Silencing of *hPar2* inhibits association of key signaling partners with the PAR_1 C-tail. **A***i* MCF7 cells stably over-expressing HA-*hPar1* and T7-Etk/Bmx were infected with a lentiviral vector driving either *sh*RNA- *hPar2* expression or a scrambled *sh*RNA-*hPar2* and cultured with or without thrombin activation (1 U/ml) (**A***i*) or the PAR_1 selective ligand, TFLLRN (100 μM) (**A***ii*). Cell lysates were collected at the indicated times and immunoprecipitated using anti-HA antibodies. Immunoprecipitates were separated on SDS-PAGE and Western blotted with anti-T7 antibody to detect T-7-tagged Etk/Bmx-T7. Etk/Bmx is seen after 15 and 20 min of thrombin treatment in cells without *hPar2* silencing (scrambled *sh*RNA-*hPar2*); but is not detectable in cells infected with *shRNA-Par2*. A specific, Etk/Bmx is seen associated after 5′, 10′, 15′, and 20 min following TFLLRN activation in cells expressing both HA-*hPar1* and endogenous *hPar2* (scrambled *sh*RNA-*hPar2*). In-contrast, the Etk/Bmx association is not detected in the presence of *shRNA-hPar2*. **B** Silencing *hPar2* inhibits thrombin-induced association between PAR_1 and Akt. MCF7 clones overexpressing HA-*hPar1*, with *sh*RNA *hPar2* silencing (*right*), or scrambled *sh*RNA *hPar2* (*left*), were treated with thrombin for the indicated times. Cell lysates were immunoprecipitated with anti-HA to precipitate HA-PAR_1 and analyzed by Western blot with anti-Akt antibodies, followed by antibodies to phosphorylated Akt (pAkt). HA-PAR_1 serves as a loading control. **C** PAR_2 expression in the MCF7 clone (expressing *hPar1*, *hPar2*, and *etk/bmx*) with and without *sh*RNA silencing as compared with a housekeeping gene GAPDH. **D** Silencing *hPar2* inhibits TFLLRN PAR_1 activation in MDA-MB-231 cells. MDA-MB-231 cells expressing high endogenous levels of both PAR_1 and PAR_2 show a similar pattern (to MCF7 cells) of selective PAR_1 inhibition in the presence of *sh*-RNA *hPar2*. TFLLRN activation induces the co-IP between PAR_1 and Akt immediately after 2′, 10′, and 20′ activation (scrambled *sh*-RNA *hPar2*). In the presence of *sh*-RNA *hPar2*, this association is markedly inhibited. β-actin serves as a loading control

down *hPar2* abrogated the association of Akt with PAR_1 C-tail, as well as its phosphorylation following thrombin activation. A scrambled *sh*RNA-*hPar2* had no effect on the complex formation between PAR_1-C-tail and Akt as also p-Akt (Fig. 1b see also Fig. S1). Similarly, empty vector transfection did not result in any co-immunoprecipitation (MCF7 cells do not express PAR_1; data not shown). The levels of *hPar1, hPar2*, Etk/Bmx, and degree of *hPar2* silencing in these clones are shown in Fig. 1c. A similar pattern of selective PAR_1 inhibition (by *sh*RNA- *hPar2*) is also observed in MDA-MB-231 cells expressing endogenously high levels of PAR_1, PAR_2, and Akt. In the presence of scrambled *sh*RNA-*hPar2*, a potent co-association between PAR_1 and Akt is observed following TFLLRN activation. This complex formation is completely abrogated in the presence of *sh*RNA- *hPar2* (Fig. 1d).

Silencing *hPAR2* significantly reduces soft agar colony formation, Matrigel invasion, and wound migration

Anchorage-independent growth in soft agar as manifested by colony formation is a well-established indicator of tumorigenicity [39, 40]. Normal cells are incapable of multiplying in a semisolid environment. Furthermore, there is a good correlation between soft-agar colony formation and the extent of tumor generation in vivo in animal models. While MDA-MB-231 cells formed very small colonies prior to activation (Fig. 2Ai, a, b; control), large colonies in soft agar were observed following treatment with thrombin (Fig. 2Ai, panel c) or with the PAR_1-specific ligand TFLLRNPNDK (Fig. 2Ai, panel d). In contrast, cells expressing *sh*RNA-GFP-*hPar2* were incapable of generating colonies following the addition of either thrombin (Fig. 2Ai, panel e, cells expressing *sh*RNA-*hPar2* visualized by GFP fluorescence) or TFLLRNPNDK (Fig. 2Ai, panel f; the small-size colonies shown, all express *sh*RNA-*hPar2* due to high lentiviral infection levels). Scrambled *hPar2* had no effect on the formation of large colonies in the presence of thrombin activation (Fig. 2Ai panel g). Cells infected with *sh*RNA- *hPar1* and thrombin activated formed small-size colonies (Fig. 2Ai panel h, as compared with panel c; for control non-silenced cells after thrombin activation). SLIGKV PAR_2-specific activation showed the formation of rather large colonies (Fig. 2Ai panels i, j). Overall, when grown on soft agar, MDA-MB-231 *sh-hPar2* cells formed significantly smaller foci and a smaller number of foci than control MDA-MB-231-activated cells. In-contrast, MDA-MB-231 cells formed significantly larger foci following PAR activation than control cells, while the number of foci remained the same. Figure 2Aii shows that infection with the *sh*RNA-*hPar2* vector decreased *h*PAR_2 expression to undetectable levels without altering *hPar1* expression. Histograms represent the mean colony area size/cm^2 under the different treatments (Fig. 2Aiii). Thus, reducing PAR_2 expression alone not only attenuates PAR_1 and PAR_2-driven cell transformation but also considerably inhibits transformation induced by the selective activation of PAR_1. The data were statistically evaluated by ANOVA Tukey HSD of multiple comparison, showing a p value of 0.004 within groups. The mean difference is significant at the 0.05 level.

Silencing of *hPar2* also inhibited significantly TFLLRN-induced invasion of MDA-MB-231 cells in a Matrigel invasion assay, while scrambled *sh*RNA-*hPar2* had no effect (Fig. 2Bi, ii). In parallel, when we analyzed Matrigel invasion in *sh hPar1* MDA-MB-231-silenced cells, we observed a marked inhibition following thrombin activation. This was not seen following SLIGKV activation, whereby potent Matrigel invasion is observed (Fig. 2Biii, iv). Therefore, the same pattern as in MCF7 cells is observed inhibiting Matrigel invasion in the presence of silenced *hPar2* but not vice versa by *sh hPar1*. We demonstrate specificity toward PAR_1 by inhibition in the presence of PAR_1 selective antagonist SCH79797 (Supplementary data Fig S3). In order to exclude the possibility that PAR_4 is involved in MDA-MB-231 cell invasion (since these cells express also PAR_4, see Supplementary data Fig. S4, C), we performed Matrigel invasion in the presence of a PAR_4 agonist, AYPGKF. As can be observed, a low level of invasion was obtained (Fig. S4, Ai, Aii). Next, we performed Matrigel invasion following thrombin activation, in the presence of tcY-NH2 (Tocris Bioscience Inc, Minneapolis, MN, USA), a PAR_4-specific antagonist. Thrombin activation induced Matrigel invasion with no significant impact of PAR_4 antagonist on the invasion level Fig. S4, Ai, Aii). Similarly, we show that the PAR_4 antagonist does not have a significant impact on Thrombin-induced co-association between PAR_1 C-tail and Akt, in MDA-MB-231 cells (Fig. S4, B). We thus conclude that PAR_2 affects PAR_1 function and the involvement of PAR_4 in this process is marginal.

Next, we looked at the effect of silencing by *sh*RNA-*hPar2* or *sh*RNA-*Par1* on the migration of tumor cells using a tissue monolayer-wound assay. Cells of the aggressive breast cancer line MDA-MB-468 (expressing high levels of PAR_1 and PAR_2; Supplementary data Fig. S5A) or PC3 prostate cancer cells (Supplementary data Fig. S5B) were infected with lentiviral vectors expressing either *sh*RNA-*hPar2* or *sh*RNA-*hPar1*. A carefully defined wound (1-cm-wide scratch) was made in confluent MDA-MB-468 cells or PC3 cells following infection and in uninfected confluent cultures. Cells were then treated with thrombin and migration of cells into the empty space was assessed over time. There was extensive cell migration in the non-infected cells, closing the gap within 24 h. In-contrast, migration was clearly attenuated in cells infected with either *sh*RNA-*hPar1* or

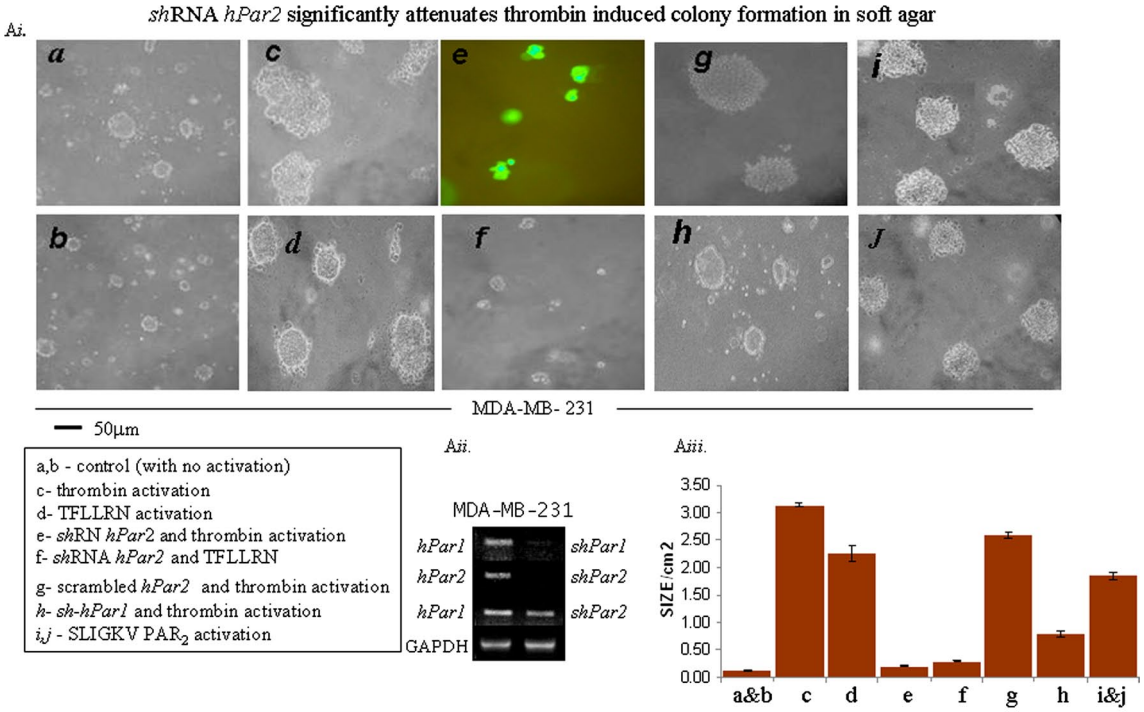

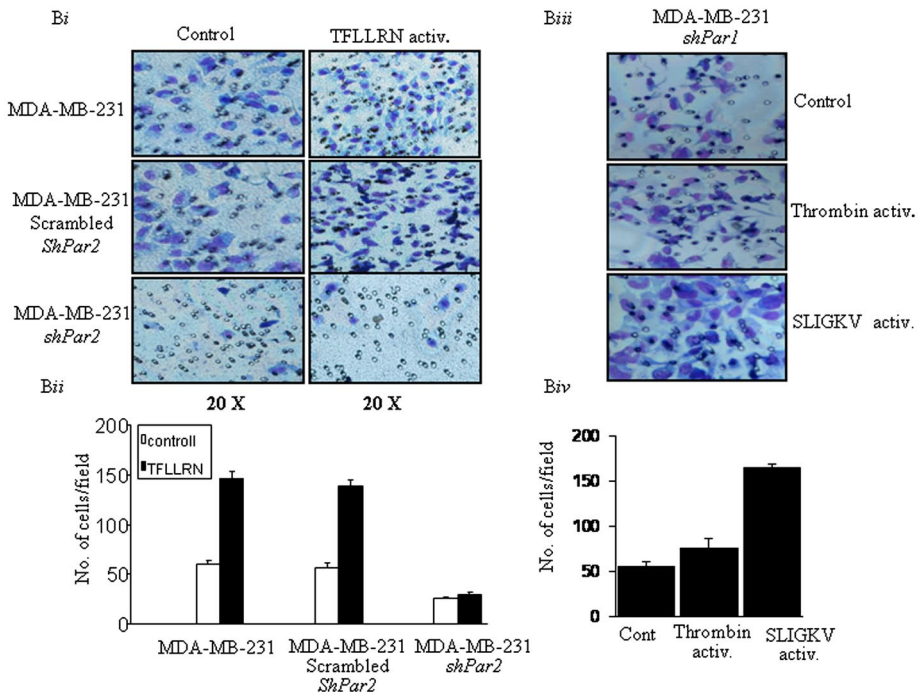

*sh*RNA-*hPar2*; *sh*RNA-*hPar2* had a more pronounced effect than *sh*RNA-*hPar1* (Fig. S5Ai, iii and S3Bi, iii, Supplementary data). When either PC3 or MDA-MB-468 cells were either infected with *sh*RNA-*hPar1* or with *sh*RNA-*hPar2,* there was no detectable expression of PAR_1 or PAR_2, respectively (Figs. S5Aii and S5Bii, Supplementary data).

Silencing of *hPar2* significantly inhibits thrombin-induced EVT cell invasion

A decisive key step in the establishment of human pregnancy is the well-orchestrated invasion of the uterus wall by specialized cells termed extravillous trophoblast (EVT). These cells are in fact a subpopulation of placenta

◀ **Fig. 2** **A***i* Silencing *hPar2* in a breast cancer cell line inhibits thrombin- or TFLLRNPNDK-induced colony formation in soft agar. 5×10^3 MDA-MB-231 cells, either uninfected (*a*, *b*) or infected with virus expressing *sh*RNA-GFP-*hPar2* (*e, f*), were plated in soft agar and activated by thrombin (*e*) or TFLLRNPNDK (*f*). Uninfected cells were treated with thrombin (*c*) or TFLLRN (*d*) as also with SLIGKV (**i**, **j**). Controls of either scrambled *sh*RNA *hPar2* with thrombin activation (*g*) and *sh*RNA *hPar1* with thrombin activation (*h*) were shown as well. After 12 days, live images were collected using a Zeiss microscope at ×20 magnification. In uninfected cells, large colonies formed following treatment with either thrombin (*c*) and somewhat smaller with TFLLRNPNDK (*d*). MDA-MB-231 cells infected with *sh*-GFP-*hPar2* formed only very small colonies after thrombin (*e*) or TFLLRNPNDK (*f*) treatment. Cells containing *sh-hPar2* are visualized by GFP fluorescence (*e*). The colonies formed under different conditions were compared with control non-activated, non-treated cells (control; *a, b*). The colonies formed in the presence of *sh*RNA-*hPar1* and after thrombin activation is significantly smaller (panel *h*) than colonies formed after thrombin activation (*c*). Scrambled *sh*RNA-*hPar2* had no effect on the colonies formed (panel *g*). Comparable colony size is obtained by SLIGKV PAR_2 activation (*i, j*) as found by TFLLRNPNDK (*d*). Images shown are representative of three independent experiments. **A***ii* RT-PCR analysis of *hPar1* and *hPar2* mRNA expression before and after *sh*RNA silencing. GAPDH levels were analyzed as a control. **A***iii* Histogram shows mean ± SE of triplicate values from three independent experiments. Post hoc evaluation of multiple comparison (ANOVA Tukey HSD) showed a *p* value of 0.004 within groups. The mean difference is significant at the 0.05 level. For ANOVA evaluation we used IBM SPSS 20.0 software. **B***i* Silencing *hPar2* in MDA-MB-231 cells inhibits TFLLRN PAR_1 invasion. Matrigel invasion in the presence of *sh*RNA-*hPar2*-infected cells as compared with scrambled *sh*RNA. While TFLLRN specific activation of PAR_1 induces Matrigel invasion in MDA-MB-231 cells, this was attenuated in the presence of *sh*RNA-*hPar2*-infected cells. In-contrast, no effect was observed when a scrambled *sh*RNA was utilized to infect the cells, demonstrating a markedly induced Matrigel invasion similar to non-treated activated parental MDA-MB-231 cells. **B***ii* Histograms represents quantification of the cells/HPF invaded the Matrigel layer. Unpaired Student's *t* test was used. This experiment is a representative of three independent experiments performed in triplicates. **B***iii* Silencing *hPar1* in MDA-MB-231 cells did mot inhibit PAR_2 function. In MDA-MB-231 cells silenced for *hPar1*, thrombin activation resulted with a low level of Matrigel invasion. In-contrast, SLIGKV PAR_2 activation under conditions of *sh-hPar1* silencing, resulted with potent Matrigel invasion. **B***iv* Histograms represents quantification of the cells/HPF invaded the Matrigel layer in *sh*RNA *hPar1* silenced cells. Unpaired Student's *t* test was used. This experiment is a representative of three independent experiments performed in triplicates

cytotrophoblast capable of forming anchoring villi that invade and reach the uterine wall thereby allowing direct contact with the maternal blood. A well-established in vitro model system based on the isolation of villi from early gestation placentas plated on Matrigel as a substitute for the extra cellular matrix (ECM) is utilized [33–36]. The advantage of this system is that cytotrophoblasts that differentiate along the invasive pathway mimic at large the development of normal early placenta villi [36]. We initiated our evaluation by comparing the depth of invasion under the different experimental conditions: infection of *sh*RNA-*hPar2*- viral vector as compared with scrambled *sh*-RNA-*hPar2* before and after either thrombin or TFLLRN or SLIGKV activation. The morphology of the villous trophoblast as well as the extra villous cell outgrowth columns in the various treatment groups is illustrated.

The EVT invasion into the Matrigel reached as deep as 110 μm, as observed by representative 5-μm serial sections of the Matrigel cast. Histological analyses of H&E staining are shown in Fig. 3a. The preparations of *sh*RNA-*hPar2* viral vector following activation of the PARs (e.g., thrombin, TFLLRN, SLIGKV) showed reduced EVT invasion, reaching levels of maximum 70 and 80 μm. In contrast, activation of PARs (e.g., thrombin and/or TFLLRN and SLIGKV), showed deeper invasion (e.g., 110 μm). The number of cells per high-power field for each of the treatments was evaluated at an equal level of invasion (60 μm), as shown in a representative histogram (Fig. 3a). A high level of invading cells was observed after either thrombin, TFLLRN, or SLIGKV activation, regardless of either before or after scrambled the *sh*RNA *hPar2* treatment. In conclusion, a significant inhibition was observed in the presence of *sh*RNA-*hPar2* lentiviral vector following the different activation treatments (e.g., thrombin, TFLLRN, and SLIGKV). The relative levels of PAR_1 and PAR_2 in the presence and absence of either *sh hPar2* or scrambled *sh hPar2* in the EVT organ culture is shown in Fig. 3c. The count/HPF data was statistically evaluated by ANOVA Tukey HSD of multiple comparison showing a *p* value of 0.0001 within groups. The mean difference is significant at the 0.05 level.

Co-localization of PAR_1 and PAR_2

It has been proposed previously that PAR_1 and PAR_2 are localized near each other on the cell membrane, enabling their activation as an intact functional unit. We examined their relative localization on breast cancer cells in situ by confocal microscopy. HEK293T cells were transfected with both HA-*hPar1* and YFP-*hPar2*. Twenty-four hours later, the cells were serum deprived for an additional 24 h and then activated with thrombin for 5 min. PAR_1 was visualized by anti-HA antibodies and Cy3-conjugated secondary antibodies or direct fluorescence detection for YFP-PAR_2. Activation showed merge co-localization of both PAR_1 and PAR_2 in the cell membranes (Fig. 4A, panels d, iv) as compared with either PAR_2 (Fig. 4A panels a, i) or HA-PAR_1 (Fig. 4A, panels b, ii). Control cells prior to activation exhibited abundant PAR_1 and PAR_2 on the cell surface, indicating that the transfection was efficient (data not shown). Cell nuclei were detected by draq 5 (Fig. 4A, panels c, iii) and gross cell morphology was detected by phase-contrast microscopy (Fig. 4A, v).

Co-localization of PAR_1 and PAR_2 was quantitated with the "Image-Pro Plus" (version 4.5) program, which can specifically calculate the extent of co-localization within a

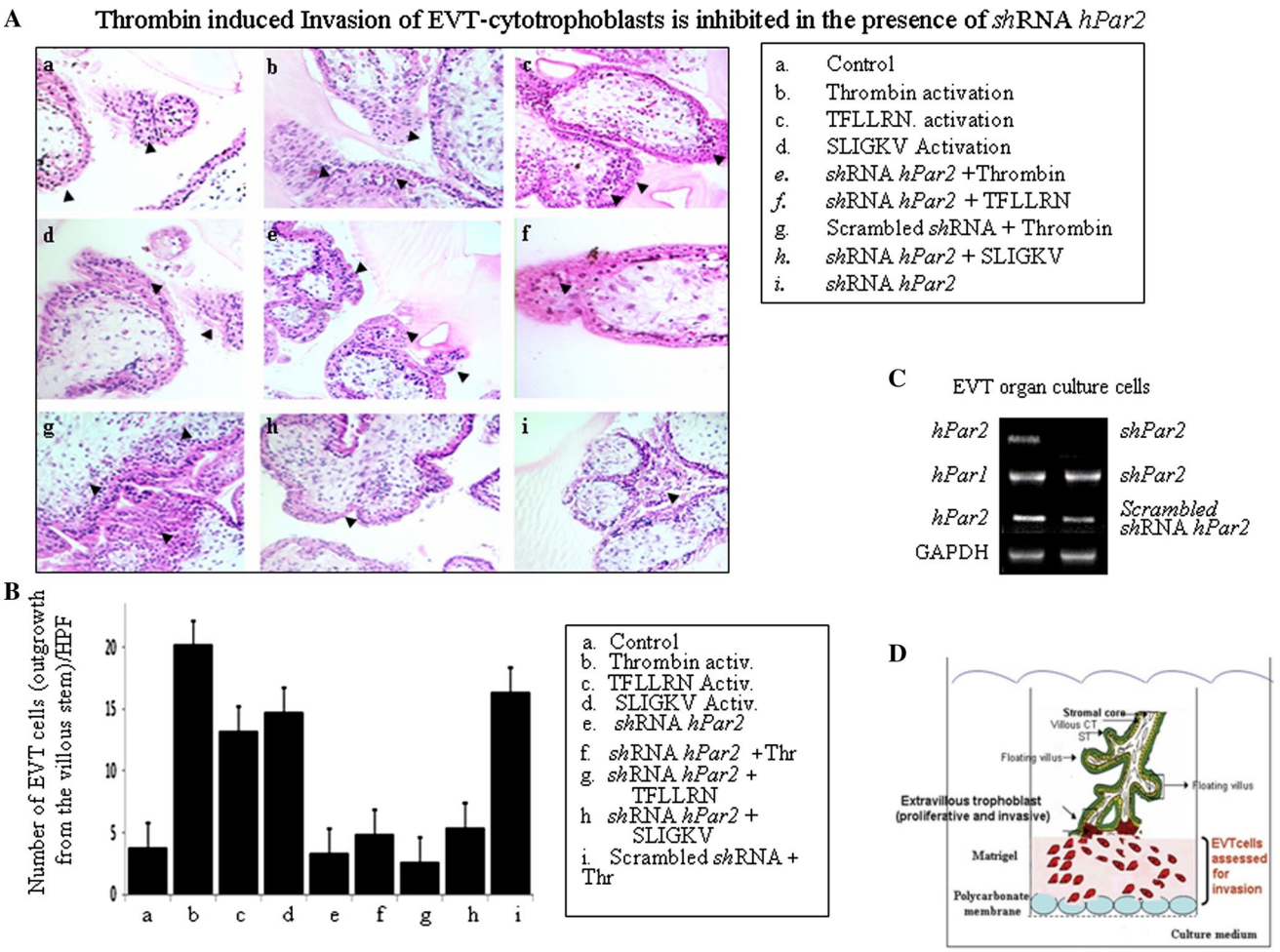

Fig. 3 Placenta-EVT organ culture invasion. **A** Morphology of EVT column growth. Invasion of placental explants of EVT-Matrigel cylinder cast after H&E staining (magnification ×20). Serial sections (5 μm each) of the Matrigel cylinder casts were embedded in paraffin blocks prepared for each of the experimental treatment conditions. Images of representative H&E-stained sections at 60-μm depth are presented. *a* Non-treated (control); *b* Thrombin (1 U/ml) activation; *c* TFLLRN (100 μM) activation; *d* SLIGKV (100 μM) activation; *e sh*RNA *hPar2* lentiviral infected EVT and thrombin (1 U/ml) activated; *f sh*RNA *hPar2* lentiviral-infected EVT and TFLLRN (100 μM) activation; *g* Scrambled *sh*RNA *hPar2* lentiviral infected EVT and thrombin (1 U/ml) activation; *h sh*RNA *hPar2* lentiviral-infected EVT and SLIKGV (100 μM) activation; *i sh*RNA *hPar2* lentiviral-infected EVTs. Note the increase in the EVT migrating cells and cell mass at the tip of the villi following either of PAR activation. In contrast, a blunt end of the villi with no sprouting cells is seen at the villi tip column in the presence of *sh*RNA *hPar2* treatment following the different activation treatment. The experiment was terminated 3 days (72 h) after EVTs treatment. Each experiment was performed using three different placentas, in triplicates. *Arrowheads* show sprouting cytotrophoblasts. **B** Quantification of EVT outgrowth cell number at 60-μm depth of invasion as shown by histogram mean values. Cells (not the villous compartment) were counted per high-power field and expressed as mean ± SEM. **C** RT-PCR analyses of PAR_1 and PAR_2 in the cultured EVTs. GAPDH serves as a control. Post hoc evaluation of multiple comparison (ANOVA Tukey HSD) showed a *p* value of 0.0001 within groups. The mean difference is significant at the 0.05 level. For ANOVA evaluation, we used IBM SPSS 20.0 software. **D** Schematic representation of EVT experimental model for invasion

defined field (co-localization is expressed using a scoring range from a low of 0.2 up to 1.0, which indicates maximal co-localization). When we used "Image Pro Plus" to analyze the HEK293T cell membrane compartment, scores of 0.97–0.98 were obtained throughout the field, indicating high co-localization between PAR_1 and PAR_2 following activation by thrombin.

To obtain direct evidence for PAR_1–PAR_2 heterodimer formation, we carried out co-immunoprecipitation analyses. For this purpose, we ectopically over-expressed HA-tagged-*hPar1* with YFP-tagged-*hPar2*. As a control, we used CXCR4, another member of the GPCR family. For this purpose, we expressed GFP-*cxcr4* in HEK293T cells along with HA-*hPar1*. The cells were treated with thrombin for 10 min and then lysed. Next, we performed immunoprecipitation using either anti-HA antibodies, or IgG (as control), separated on SDS-PAGE and Western blotted with anti-GFP antibodies. PAR_2 were detected in the

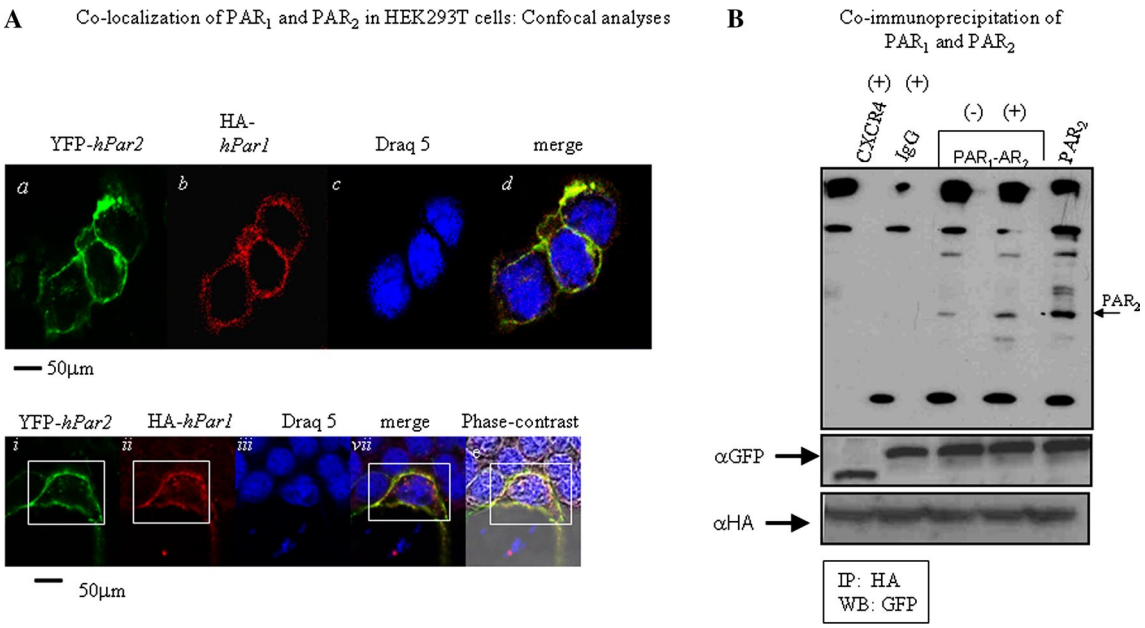

Fig. 4 Co-localization of PAR$_1$ and PAR$_2$. **A** Confocal immunofluorescence analysis. HEK-293T cells were transfected with both HA-*hPar1* and YFP-*hPar2*. After 24 h, the cells were serum deprived for an additional 24 h then activated with thrombin for 5 min followed by fixation with cold methanol. PAR$_2$ was visualized by direct fluorescence (*a*) and PAR$_1$ was visualized by immunostaining with anti HA-antibodies followed by Cy3-conjugated IgG secondary antibodies (*b*). Merge staining for both PAR$_1$ and PAR$_2$ revealed co-localization confined to the cell membrane (*d*). For reference, staining of cell nuclei with Draq5 is shown (*c*). The *bottom panel* highlights staining in one cell exhibiting the expression of YFP-*hPar2* and HA-*hPar1* on the cell membrane prior to activation (*i, ii*). Significant co-localization recapitulated by merge fluorescence is observed following five minutes thrombin activation (*iv*). This is detected as compared with cell nuclei staining (*iii*) and phase-contract analysis (*v*). The percent of positive cells for HA-*hPar1* was 58 % ± 1.2 and for YFP-*hPar2* were 55 % ± 1.86; PAR$_1$-PAR$_2$ merge was observed in 45 % ± 2.1. **B** PAR$_1$ and PAR$_2$ co-immunoprecipitate. HEK 293T cells expressing either HA-*hPar1*, YFP-*hPar2* or GFP-CXCR4 were treated with thrombin for 10 min and lysed. Cell lysates were then immunoprecipitated before (−) and after (+) thrombin activation by anti HA or IgG, resolved by SDS-PAGE and immunoblotted as indicated (by anti-GFP). While no specific complex is formed when CXCR4 and PAR$_1$ were co-IP (following 10-min thrombin activation), a specific complex is observed between PAR$_1$ and PAR$_2$ following activation. No specific band is seen when IgG were applied in the immunoprecipitation assay. Expression of CXCR4, PAR$_2$ (as indicated by anti-GFP, *first lane*), and PAR$_1$ (as shown by anti-HA) were shown as controls for transfection efficiency. The figure shown is a representative of three independent experiments

immunoprecipitates after thrombin activation; (+) as compared to PAR$_2$ levels prior to activation; (−) and similar to the position of PAR$_2$ in cell lysates expressing only PAR$_2$ (PAR$_2$) (Fig. 4B). No association was seen in cells expressing GFP-*cxcr4* or following immunoprecipitation with IgG. These results provide supporting evidence that a specific complex is formed between PAR$_1$ and PAR$_2$ following activation, but not with PAR$_1$ and CXCR4.

Modulation of PAR$_1$-PAR$_2$ induced breast tumors by a truncated PAR$_2$

The basis for this study is the concept that PAR$_1$ and PAR$_2$ act together as a functional unit in response to thrombin application, based on the close proximity position enabling the formation of heterodimers or hetero-oligomers. Knocking down of PAR$_2$ considerably attenuated the response to pro-tumor processes induced either by thrombin or the specific PAR$_1$ ligand. We therefore sought to examine the effect of a truncated form of PAR$_2$ (PAR$_2$ lacking the cytoplasmic tail) both in vitro and in vivo on PAR$_1$ tumor growth (for characterization of truncated *hPar2* cell surface expression, see Supplementary data, Fig. S6). For this purpose, we have utilized HU cells, nearly normal breast epithelial cells that do not express neither *hPar1* nor *hPar2* (see Supplementary data; Fig. S4, C). Toward this, we generated stable clones of HU cells over-expressing the following plasmids. A clone expressing HA-tagged *hPar1,* T7-tagged-Etk/Bmx and *wt hPar2*; another clone expressing HA-tagged *hPar1,* T7-tagged-Etk/Bmx and a truncated *hPar2*; a clone of *hPar2* alone or a clone expressing empty vector alone. The association between Etk/Bmx and PAR$_1$ C-tail in these clones was first analyzed. Cell lysates were processed and immunoprecipitated with anti-HA antibodies, followed by Western-blot detection of the T7-tagged-Etk/Bmx immunocomplex with anti-T7 antibody. Etk/Bmx was detected with HA-tagged PAR$_1$ in cells co-transfected with *wt hPar1* and *hPar2* following 10 min

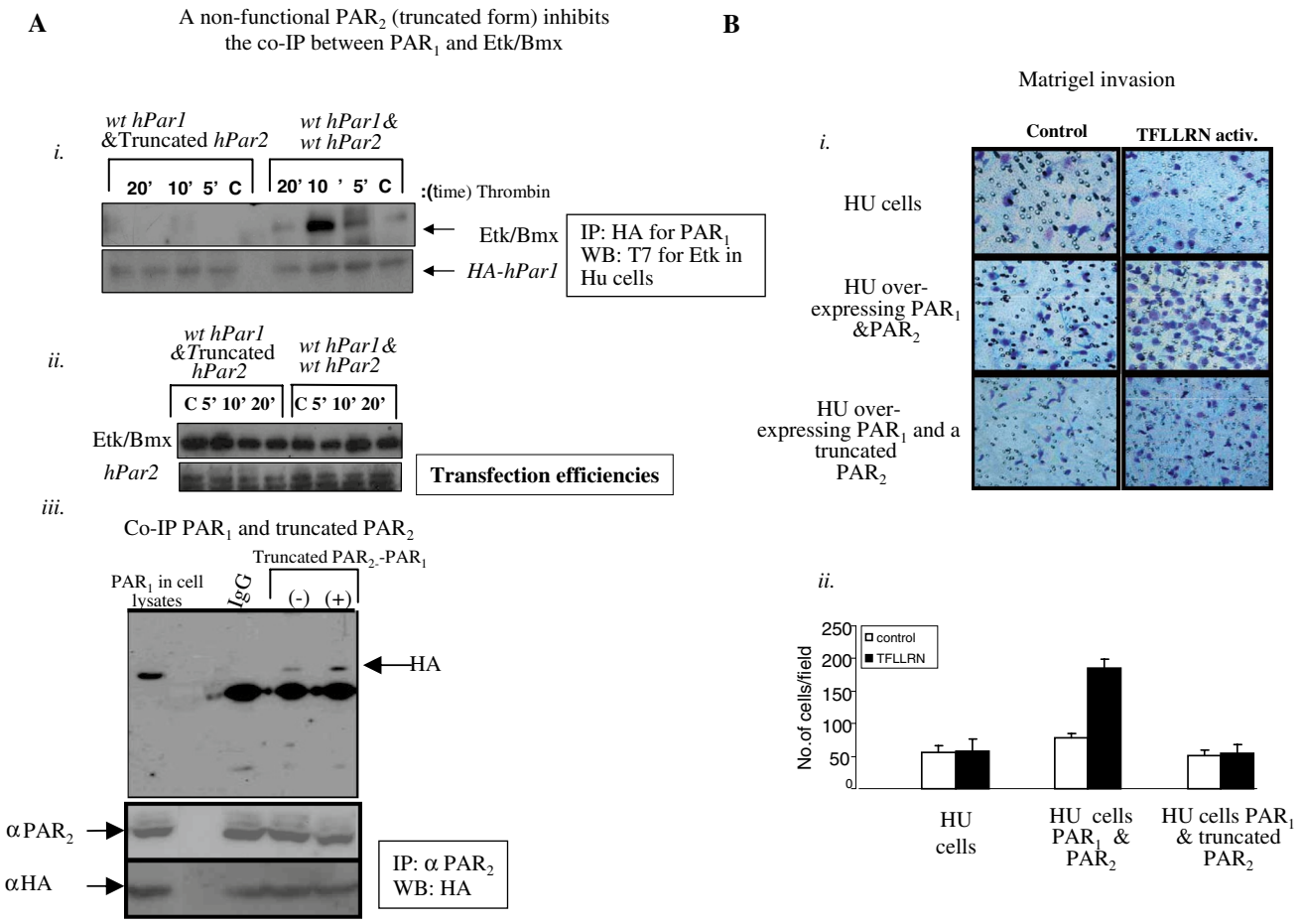

Fig. 5 **A** A truncated form of *hPar2* (devoid of C-tail) impairs PAR_1 C-tail tail ability to associate with Etk/Bmx following thrombin activation. *i* HU stable clones over-expressing either *hPar1&hPar2* or *hPar1* and a truncated form of *hPar2,* also expressing T7-*etk/bmx*, were immunoprecipitated using anti-HA antibodies to immunoprecipitate HA-PAR_1. The PAR_1 immunoprecipitates were analyzed by Western blot with anti-T7 antibodies to detect T7-tagged Etk/Bmx. Anti-HA blotting is shown as a loading control. Plasmid expression levels in the various clones are indicated (*ii*). Clones expressing HA-*hPar2* and T7-*etk/bmx* were analyzed for transfection efficiency (*iii*). PAR_1 co-immunoprecipitates with a truncated PAR_2 form. HEK 293T cells expressing HA-*hPar1* and a truncated PAR_2 form were treated with thrombin for 10 min and then lysed. Cell lysates before (−) and after (+) thrombin activation were then immunoprecipitated by either anti-PAR_2 antibodies (SAM11; Santa Cruz, CA, USA) or IgG, resolved by SDS-PAGE and immunoblotted as indicated (by anti-HA abs). While no specific band is seen when IgG was used as a control, increased PAR_1 is observed following thrombin activation (+) as compared to levels before activation (−). In lysates expressing *hPar,* blotting with anti-HA antibodies indicate the position of PAR_1 (e.g., PAR_1). Levels of truncated PAR_2 are indicated by anti PAR_2 antibodies (directed to the N-terminus of PAR_2). Anti-HA was shown for PAR_1 transfection levels. This experiment is a representative of three independent experiments. **B** Matrigel invasion induced by selective PAR_1 activation. Matrigel invasion is induced by TFLLRN treatment of HU clones over-expressing *hPar1* and *hPar2*. In contrast, TFLLRN fails to induce Matrigel invasion in cells over-expressing *hPar1* and a truncated form of PAR_2. Images are taken at ×20 magnification. Histograms representing the extent of Matrigel invasion are shown. Unpaired Student's *t* test was used. This experiment is a representative of three independent experiments performed in triplicates. *Error bars*, ± SD; $^{**}p < 0.007$

of thrombin activation. In contrast, in the clone expressing *hPar1* and a truncated form of *hPar2*, thrombin treatment elicited a markedly less association between PAR_1 C-tail and Etk/Bmx (Fig. 5A). The levels of Etk/Bmx, truncated PAR_2, and *HA-hPar1* expression is shown (Fig. 5Aii). This finding suggests that the presence of truncated PAR_2, lacking the cytoplasmic C-tail inhibits PAR_1-PAR_2 functional activity. We further demonstrate that the truncated form of PAR_2 co-immunoprecipitates with PAR_1. For this purpose, we have used HEK293T cells expressing HA-*hPar1* and truncated form of PAR_2. The cells were treated for 10 min with thrombin (+), lysed, and immunoprecipitated using anti-PAR_2 or IgG (as control). Western-blot analysis using anti-HA antibodies showed the presence of PAR_1 in the PAR_2 immunoprecipitates following thrombin activation but not prior to activation (−), or by the use of IgG. The position of PAR_1 in the blot is compared with PAR_1 size obtained in the cell lysates (Fig. 5Aiii). Hence, the truncated form of PAR_2 is well expressed on the cell-surface (Supplementary data, Fig. S6) presumably in a close

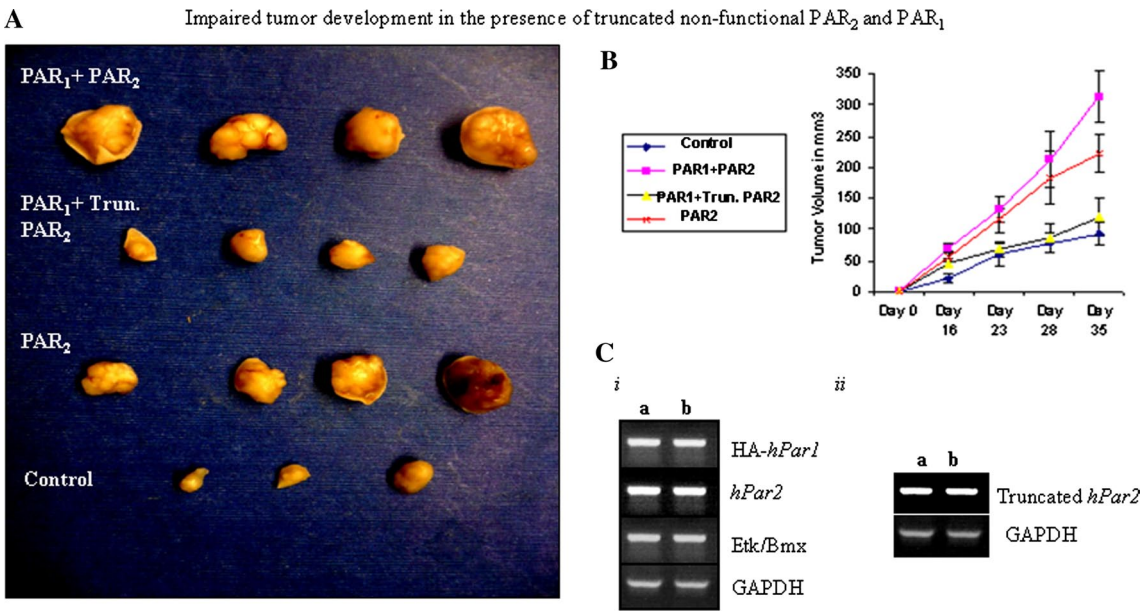

Fig. 6 Impaired tumor development in the presence of PAR$_1$ and truncated PAR$_2$. Stable clones of HU cells expressing either *hPar2* or *hPar1* and *hPar2*, or *hPar1* and truncated *hPar2* were injected subcutaneously into nude mice (2×10^6 cell/mouse). Parental non-transfected HU cells were used as a control. **A** Tumor morphological appearance. Mice injected either with *hPar1* and *hPar2 or hPar2* developed tumors at the sites of injection. In-contrast, mice inoculated with *wt hPar1* and a truncated form of *hPar2* did not develop or developed very little tumors (*a*). By the end of the experiment (e.g., 35 days) the mice were killed and the tumors were excised, measured, and weighed ($n = 4$/per group). **B** Mouse tumor growth curve in nude mice. Tumors were excised, weighed and measured at the indicated times and tumor volume (mm^3) was calculated. *Error bars* show SD; * indicates $p < 0.006$. Data shown are representative of three experiments performed. **C***i, ii* RT-PCR analyses of the indicated clones (*a* and *b*; two different clones) show the expression of PAR$_1$ and PAR$_2$, truncated PAR$_2$ and the prime signal protein Etk/Bmx

proximity with PAR$_1$, and upon activation forms a complex with PAR$_1$.

In a Matrigel invasion assay, selective activation of PAR$_1$ with TFLLRN considerably enhanced the invasion of HU cells over-expressing both PAR$_1$ and PAR$_2$. This PAR$_1$-induced invasion was noticeably inhibited in clones stably expressing PAR$_1$ and the truncated form of PAR$_2$ (Fig. 5Bi, ii).

Noticeably, TFLLRN activates specifically PAR$_1$, but not PAR$_2$ (see Supplementary data Figs. S8, S9). When the PAR$_2$ mutant R36A, incapable of extra-cellular cleavage by trypsin for activation was silenced, a marked inhibition of TFLLRN PAR$_1$ induced Matrigel invasion (Supplementary data Fig. S9) was observed. Hence, the physical presence of PAR$_2$ in a non-activated state is sufficient and required in close proximity for PAR$_1$ function. When the clone expressing *wt hPar1* and a truncated form of *hPar2* were re-infected with *wt hPar2*, a complete rescue was observed after TFLLRN activation showing a potent Matrigel invasion properties (Supplementary data, Fig. S7).

The various clones (e.g., *wthPar2, hPar1&hPar2*, *hPar1*, and truncated *hPar2*), were then inoculated subcutaneously into nude mice. The mice were monitored for 35 days (at which time the tumors became noticeable), killed, and tumors were collected and embedded in paraffin. While minimal to nearly no tumors were seen following injection of the parental HU cells, large tumors were observed after injection of HU clones over-expressing *hPar1* and *hPar2* (as well as the prime signal protein; T7-tagged-Etk/Bmx), similar to the tumors obtained following inoculation of cells expressing *hPar2* alone. In the presence of *hPar1* and a truncated form of *hPar2*, considerably smaller tumors were seen (Fig. 6A, B). These tumors were also significantly smaller than PAR$_1$-driven tumors (data not shown). The levels of tag-PAR$_1$, *wt* PAR$_2$ and truncated PAR$_2$ expression in two clones are shown (Fig. 6C).

Together, the in vitro and in vivo effects of introducing a truncated PAR$_2$ indicate that truncated PAR$_2$ has an inhibitory effect on PAR$_1$/PAR$_2$-induced tumor-promoting processes similar to the inhibition seen following *sh*RNA silencing.

Discussion

It has been shown that PAR$_1$ transactivates PAR$_2$ donating its cleaved new N-terminal domain to bind inter-molecularly and activate in trans PAR$_2$ [26, 27]. Ample evidence has been gathered since the first demonstration by O'Brien et al. [26] showing conclusively that PAR$_1$-tethered ligands can transactivate PAR$_2$ and provide a full agonist for its function. This takes place in vivo as shown by Kaneider

et al. [24] that PAR_2 associates with PAR_1 and switches thrombin-induced endothelial cell from a barrier disruption function to a protective role. In another work, PAR_2 expression was shown necessary for PAR_1-induced hyperplasia in mouse models [28]. Recently, an in-depth work by the group of Trejo JA showed that the internalization trafficking machinery of PAR_1–PAR_2 heterodimer differs from PAR_1 trafficking [29]. Albeit, the molecular mechanisms that regulate PAR_1–PAR_2 heterodimer formation, signaling, and trafficking are not yet known.

In the present study, we show that PAR_1 and PAR_2 act as a functional unit in promoting breast cancer. We found that PAR_1-induced breast tumor development and the corresponding signaling events are markedly inhibited when PAR_2 expression is either knocked-down or lacking the C-tail portion. Hence, PAR_2 must be present for a wide spectrum of tumorigenic activities and for the initiation of PAR_1 early signaling events but not vice versa.

Our studies confirm the close proximity of PAR_1 and PAR_2, which leads to co-localization following appropriate activation. This was demonstrated by both confocal image analysis and co-immunoprecipitation of PAR_1–PAR_2 forming a complex as shown following the ectopic over-expression of either GFP-cxcr4, HA-*hPar1*, and YFP-*hPar2* plasmids. While specific co-immunoprecipitation is seen between HA-*hPar1* and YFP-*hPar2*, no such complex is observed when GFP-cxcr4 and HA-*hPar1* are used. Certainly, the truncated form of PAR_2 is also found localized in close proximity with PAR_1 allowing a potent complex formation. The physiological significance of the presence of PAR_2 cytoplasmic C-tail is demonstrated in a xenograft mouse model for tumor development, showing a markedly reduced tumor formation when a truncated *hPar2* is present.

Our findings are in line with the elegant studies by Sevigny et al. on PAR_1/PAR_2-driven hyperplasia in medial and neointimal arterial SMC growth [28, 41], and support preceding work from this group and others on PAR_1 and PAR_2 trans-activation [25, 27]. It is not surprising that silencing of PAR_2 reduces functional outcomes of PAR_1/PAR_2-driven tasks. However, the marked inhibition of a selective PAR_1-initiated activities, previously shown by the PAR_1-P1pal-13 intracellular specific activation [28, 41] and in the present study by TFLLRNPNDK, is not fully understood and needs further exploration. PAR_2 was found inactivated in the VSMC system, suggesting that the physical presence of PAR_2 is important even in the non-activated state. We present now data showing that the physical close proximity of PAR_2 is sufficient and required for PAR_1 selective function. When a mutant of PAR_2 (R36A) that is not activated by trypsin was silenced by *sh*RNA-*hPar2,* a marked inhibition of TFLLRN induced Matrigel invasion was obtained. In parallel, we demonstrate that while trypsin effectively induced PAR_2-driven Matrigel invasion, TFLLRN had no effect resulting with null to very little PAR_2-induced Matrigel invasion (see Supplementary data Figs S8, S9). Hence, the presence of PAR_2 is required for PAR_1 function also in a non-activated state. More specifically, it is suggested that the presence of PAR_2 C-tail is essential, although this role needs yet to be further elucidated. The functional dependence of PAR_1 on PAR_2 may be due to the formation of heterodimers or oligomers, as shown in other cell types. However, it is also possible that PAR_2 has a dominating regulatory effect on PAR_1 in a manner that has not yet been discovered. Interestingly, recently it has been demonstrated that PAR_1 drives the trafficking behavior of PAR_2 [29]. In addition, the current data do not rule out the possibility that PAR_2 acts through a third, yet unknown, partner that is necessary for PAR_1 efficient activity. The fact that a truncated PAR_2 inhibits PAR_1 suggests that there is essential signaling cross-talk between PAR_1 and PAR_2.

Along this line of evidence, a different signaling interface was shown by PAR_1-PAR_2 heterodimers [29]. Thrombin-induced internalization trafficking indicates that PAR_1–PAR_2 heterodimer stability leads to a conformational change that allows co-internalization and β-arrestin recruitment, an event that is not observed by activated PAR_1 (which rather binds the clathrin adaptor; AP-2) [42]. The β-arrestin recruitment to PAR_1-PAR_2 heterodimer occurs through a distinct interface and elicits a unique signaling response that is different from signaling by PAR_1 alone. Therefore, thrombin PAR_1-PAR_2 dimer formation results in a biased response elicited by β-arrestins. We have previously demonstrated that PAR_1 promotes the binding of β-arrestin-2 to disheveled (DVL), suggesting a role for β-arrestin-2 in PAR_1-induced DVL phosphorylation dynamics and β-catenin stabilization [43]. It remains to elucidate whether thrombin PAR_1–PAR_2 formation evokes a biased pro-tumor signaling event that represents a different interface than either PAR_1 or PAR_2 alone.

In fact, it was demonstrated [29] that activated PAR_2 requires its C-tail for the stable association with β-arrestins but not for internalization, whereby a truncated form of PAR_2 effectively internalizes [44]. Indeed, the PAR_2 C-tail is not required or necessary for thrombin-induced β-arrestin recruitment to the PAR_1–PAR_2 on the endosomes. Hence, it appears that the truncated PAR_1–PAR_2 dimer internalizes similar to PAR_1–PAR_2 and recruits β-arrestins. Notably, we provide the first demonstration in the context of cancer that the use of a truncated form of PAR_2 attenuates PAR_1-driven pro-tumor function in vitro and in vivo.

It is also not clear whether activation of PARs leads to homodimer as well as heterodimer formation is not clear. It was previously suggested, based on BRET2 analysis, that both PAR_1–PAR_3 heterodimers and PAR_1–PAR_1

homodimers are formed in vascular endothelial cells and induce distinct signaling repertoires: PAR_1–PAR_3 heterodimers appeared to be selectively coupled to Gα13 as compared with the PAR_1–PAR_1 homodimer, which coupled to both $G_{\alpha q}$ and $G_{\alpha}13$ [22].

Formation of heterodimeric receptors most likely allows a broader range of activation outcomes and more complex regulation than obtained with a monomer. In the case of PAR_1 and PAR_2, a broader G-protein response may be observed as PAR_1 functions via $G_{\alpha 12/13}$ and PAR_2 via $G_{\alpha q}$, $G_{\alpha 11}$, $G_{\alpha 19}$, $G_{\alpha 12}$, and $G_{\alpha 13}$ [45]. However, Etk/Bmx is immobilized onto the PAR_1 C-tail as an early key partner [37], and we find a similar association of Etk/Bmx with PAR_2-C-tail following activation (Kancharla et al., manuscript in preparation). This suggests that in the heterodimeric status when the two C-tails are in close proximity, the amplification of an early signal associating partner rather takes place and not expansion to additional signaling partners. At the present time, the possibility that the heterodimers affect receptor internalization and trafficking cannot be ruled out [46] and was recently addressed [29].

Emerging data appointed PAR_2 with a major role in breast cancer development. This is based among others, on the observed delay in the onset of tumors, following intercross between PAR_2 knock-out mice and polyoma middle T (PyMT) mammary gland mouse model for spontaneous tumor growth but not via the intercross with $PAR_1^{-/-}$mouse [47]. Although this was observed in one mouse model, it may suggest that PAR_2 plays a dominant role and drives pro-tumor function. This PAR_2 pro-tumor function may be initiated by another coagulation component, tissue factor (TF), since TF cytoplasmic domain-deleted mice have been shown also to delay the spontaneous breast cancer development in the polyoma middle T model [48].

A similar approach to assess the relative contribution of PAR_1 and PAR_2 in breast cancer was taken previously [49]; those studies used *sh*RNA silencing of PAR_1 or PAR_2 and revealed a significant role of PAR_2 in the process. Like PAR_1, PAR_2 was first identified as a cell receptor activated by FVIIa and Xa enzymes of the coagulation/hemostasis system. The location of FVIIa and Xa upstream of thrombin in the coagulation cascade suggests cross-talk and sequential trans-activation of PAR_1 and PAR_2 in breast cancer [49]. Our study is novel in demonstrating the significance of PAR_2 C-tail rather than silenced expression. This was shown both in tumor-associated processes as well as in a physiological invasion procedure.

The placenta is characterized by extensive invasion of cytotrophoblasts into the uterus wall, thereby allowing a direct contact of cytotrophoblasts with the maternal blood [30–32]. It is well recognized that trophoblast invasion during the first trimester is a critical step in the establishment of human pregnancy outcome. We as well as others have demonstrated that PAR family members are spatially expressed along the invasive process of early human trophoblast development [50, 51]. While previously we have assessed PAR_1 and PAR_2 activation, β-catenin stabilization and invasion in the EVT organ-culture system [33], we now demonstrate that *sh*RNA *hPar2* silencing, following lentiviral infection significantly inhibits both the thrombin-induced and selective TFLLRN PAR_1 activated EVT invasion. Hence, also in a highly regulated, spatial and time-limited physiological invasion process, the presence of *hPar2* is essential. The outcome of these findings points out the importance of PAR_2 during placenta implantation to the uterus deciduas. This may suggest that proper anchoring of the placenta to uterus deciduas may require PAR_2.

As the number of reports demonstrating GPCR dimerization has recently increased enormously, it is becoming well established that most GPCRs form either homo- or hetero-oligomers. PARs are no exception to this principle, acting predominantly as heterodimers in several combinations (PAR_1 and PAR_3, PAR_1 and PAR_4, as well as PAR_1 and PAR_2). Other GPCRs, including the chemokine receptors CCR2 and CCR5, have been shown to form both homo- and heterodimers [21], as have CCR2 and CXCR4.

In the present study, we demonstrate that PAR_1 and PAR_2 act together as one functional unit in tumor biology and show that PAR_2 C-tail is important for PAR_1 activities by a mechanism that remains to be elucidated. Our findings suggest that the PAR_1-PAR_2 system will be the focus of future novel therapies in breast cancer treatment.

Acknowledgments We are grateful to Dr. Susan Lewis for editing the manuscript. This work was supported by grants from the Israel Science Foundation, and Nofar Chief Israeli Scientist, Trade and Industrial Office (to Bar-Shavit, R).

Conflict of interest There are no potential conflicts of interest to disclose.

References

1. Takeda S, Kadowaki S, Haga T, Takaesu H, Mitaku S (2002) Identification of G protein-coupled receptor genes from the human genome sequence. FEBS Lett 520:97–101
2. Fredriksson R, Lagerstrom MC, Lundin LG, Schioth HB (2003) The G-protein-coupled receptors in the human genome form five main families. Phylogenetic analysis, paralogon groups, and fingerprints. Mol Pharmacol 63:1256–1272
3. Kolakowski LF Jr (1994) GCRDb: a G-protein-coupled receptor database. Receptors Channels 2:1–7
4. Bockaert J, Pin JP (1999) Molecular tinkering of G protein-coupled receptors: an evolutionary success. EMBO J 18:1723–1729
5. Lagerstrom MC, Schioth HB (2008) Structural diversity of G protein-coupled receptors and significance for drug discovery. Nat Rev 7:339–357
6. Vu TK, Hung DT, Wheaton VI, Coughlin SR (1991) Molecular cloning of a functional thrombin receptor reveals a novel proteolytic mechanism of receptor activation. Cell 64:1057–1068

7. Stenkamp RE, Teller DC, Palczewski K (2002) Crystal structure of rhodopsin: a G-protein-coupled receptor. ChemBioChem 3:963–967
8. Swift S, Leger AJ, Talavera J, Zhang L, Bohm A, Kuliopulos A (2006) Role of the PAR1 receptor 8th helix in signaling: the 7-8-1 receptor activation mechanism. J Biol Chem 281:4109–4116
9. Kenakin T (2001) Inverse, protean, and ligand-selective agonism: matters of receptor conformation. Faseb J 15:598–611
10. Kenakin T (2011) Functional selectivity and biased receptor signaling. J Pharm Exp Ther 336:296–302
11. Reiter E, Ahn S, Shukla AK, Lefkowitz RJ (2012) Molecular mechanism of beta-arrestin-biased agonism at seven-transmembrane receptors. Annu Rev Pharmacol Toxicol 52:179–197
12. Cherezov V, Rosenbaum DM, Hanson MA, Rasmussen SG, Thian FS, Kobilka TS, Choi HJ, Kuhn P, Weis WI, Kobilka BK, Stevens RC (2007) High-resolution crystal structure of an engineered human beta2-adrenergic G protein-coupled receptor. Science 318:1258–1265
13. Warne T, Serrano-Vega MJ, Baker JG, Moukhametzianov R, Edwards PC, Henderson R, Leslie AG, Tate CG, Schertler GF (2008) Structure of a beta1-adrenergic G-protein-coupled receptor. Nature 454:486–491
14. Jaakola VP, Griffith MT, Hanson MA, Cherezov V, Chien EY, Lane JR, Ijzerman AP, Stevens RC (2008) The 2.6 angstrom crystal structure of a human A2A adenosine receptor bound to an antagonist. Science 322:1211–1217
15. Hanson MA, Cherezov V, Griffith MT, Roth CB, Jaakola VP, Chien EY, Velasquez J, Kuhn P, Stevens RC (2008) A specific cholesterol binding site is established by the 2.8 a structure of the human beta2-adrenergic receptor. Structure 16:897–905
16. Chien EY, Liu W, Zhao Q, Katritch V, Han GW, Hanson MA, Shi L, Newman AH, Javitch JA, Cherezov V, Stevens RC (2010) Structure of the human dopamine D3 receptor in complex with a D2/D3 selective antagonist. Science 330:1091–1095
17. Wu B, Chien EY, Mol CD, Fenalti G, Liu W, Katritch V, Abagyan R, Brooun A, Wells P, Bi FC, Hamel DJ, Kuhn P, Handel TM, Cherezov V, Stevens RC (2010) Structures of the CXCR4 chemokine GPCR with small-molecule and cyclic peptide antagonists. Science 330:1066–1071
18. Wu H, Wacker D, Mileni M, Katritch V, Han GW, Vardy E, Liu W, Thompson AA, Huang XP, Carroll FI, Mascarella SW, Westkaemper RB, Mosier PD, Roth BL, Cherezov V, Stevens RC (2012) Structure of the human kappa-opioid receptor in complex with JDTic. Nature 485:327–332
19. Hereld D, Jin T (2008) Slamming the DOR on chemokine receptor signaling: heterodimerization silences ligand-occupied CXCR4 and delta-opioid receptors. Eur J Immunol 38:334–337
20. Mellado M, Rodriguez-Frade JM, Vila-Coro AJ, Fernandez S, de Martin Ana A, Jones DR, Toran JL, Martinez AC (2001) Chemokine receptor homo- or heterodimerization activates distinct signaling pathways. EMBO J 20:2497–2507
21. Sohy D, Parmentier M, Springael JY (2007) Allosteric transinhibition by specific antagonists in CCR2/CXCR4 heterodimers. J Biol Chem 282:30062–30069
22. McLaughlin JN, Patterson MM, Malik AB (2007) Protease-activated receptor-3 (PAR3) regulates PAR1 signaling by receptor dimerization. Proc Natl Acad Sci USA 104:5662–5667
23. Leger AJ, Jacques SL, Badar J, Kaneider NC, Derian CK, Andrade-Gordon P, Covic L, Kuliopulos A (2006) Blocking the protease-activated receptor 1-4 heterodimer in platelet-mediated thrombosis. Circulation 113:1244–1254
24. Kaneider NC, Leger AJ, Agarwal A, Nguyen N, Perides G, Derian C, Covic L, Kuliopulos A (2007) 'Role reversal' for the receptor PAR1 in sepsis-induced vascular damage. Nat Immunol 8:1303–1312
25. Nystedt S, Ramakrishnan V, Sundelin J (1996) The proteinase-activated receptor 2 is induced by inflammatory mediators in human endothelial cells. Comparison with the thrombin receptor. J Biol Chem 271:14910–14915
26. O'Brien PJ, Prevost N, Molino M, Hollinger MK, Woolkalis MJ, Woulfe DS, Brass LF (2000) Thrombin responses in human endothelial cells. Contributions from receptors other than PAR1 include the transactivation of PAR2 by thrombin-cleaved PAR1. J Biol Chem 275:13502–13509
27. Blackhart BD, Emilsson K, Nguyen D, Teng W, Martelli AJ, Nystedt S, Sundelin J, Scarborough RM (1996) Ligand cross-reactivity within the protease-activated receptor family. J Biol Chem 271:16466–16471
28. Sevigny LM, Austin KM, Zhang P, Kasuda S, Koukos G, Sharifi S, Covic L, Kuliopulos A (2012) Protease-activated receptor-2 modulates protease-activated receptor-1-driven neointimal hyperplasia. Arterioscler Thromb Vasc Biol 31:e100–e106
29. Lin H, Trejo J (2013) Transactivation of the PAR1-PAR2 heterodimer by thrombin elicits beta-arrestin-mediated endosomal signaling. J Biol Chem 288:11203–11215
30. Cross JC, Baczyk D, Dobric N, Hemberger M, Hughes M, Simmons DG, Yamamoto H, Kingdom JC (2003) Genes, development and evolution of the placenta. Placenta 24:123–130
31. Cross JC, Werb Z, Fisher SJ (1994) Implantation and the placenta: key pieces of the development puzzle. Science 266:1508–1518
32. Aplin JD, Straszewski-Chavez SL, Kalionis B, Dunk C, Morrish D, Forbes K, Baczyk D, Rote N, Malassine A, Knofler M (2006) Trophoblast differentiation: progenitor cells, fusion and migration: a workshop report. Placenta 27(Suppl A):S141–S143
33. Grisaru-Granovsky S, Maoz M, Barzilay O, Yin YJ, Prus D, Bar-Shavit R (2009) Protease activated receptor-1, PAR1, promotes placenta trophoblast invasion and beta-catenin stabilization. J Cell Physiol 218:512–521
34. Genbacev O, Schubach SA, Miller RK (1992) Villous culture of first trimester human placenta–model to study extravillous trophoblast (EVT) differentiation. Placenta 13:439–461
35. Bose P, Kadyrov M, Goldin R, Hahn S, Backos M, Regan L, Huppertz B (2006) Aberrations of early trophoblast differentiation predispose to pregnancy failure: lessons from the anti-phospholipid syndrome. Placenta 27:869–875
36. Bischof P, Irminger-Finger I (2005) The human cytotrophoblastic cell, a mononuclear chameleon. Int J Biochem Cell Biol 37:1–16
37. Cohen I, Maoz M, Turm H, Grisaru-Granovsky S, Maly B, Uziely B, Weiss E, Abramovitch R, Gross E, Barzilay O, Qiu Y, Bar-Shavit R (2010) Etk/Bmx regulates proteinase-activated-receptor1 (PAR1) in breast cancer invasion: signaling partners, hierarchy and physiological significance. PLoS ONE 5:e11135
38. Hollenberg MD, Saifeddine M, al-Ani B, Kawabata A (1997) Proteinase-activated receptors: structural requirements for activity, receptor cross-reactivity, and receptor selectivity of receptor-activating peptides. Can J Physiol Pharmacol 75:832–841
39. Colburn NH, Bruegge WF, Bates JR, Gray RH, Rossen JD, Kelsey WH, Shimada T (1978) Correlation of anchorage-independent growth with tumorigenicity of chemically transformed mouse epidermal cells. Cancer Res 38:624–634
40. Dodson MG, Slota J, Lange C, Major E (1981) Distinction of the phenotypes of in vitro anchorage-independent soft-agar growth and in vivo tumorigenicity in the nude mouse. Cancer Res 41:1441–1446
41. Pawlinski R, Holinstat M (2011) We can do it together: PAR1/PAR2 heterodimer signaling in VSMCs. Arterioscler Thromb Vasc Biol 12:2775–2776
42. Paing MM, Johnston CA, Siderovski DP, Trejo J (2006) Clathrin adaptor AP2 regulates thrombin receptor constitutive internalization and endothelial cell resensitization. Mol Cell Biol 26:3231–3242

43. Turm H, Maoz M, Katz V, Yin YJ, Offermanns S, Bar-Shavit R (2010) Protease-activated receptor-1 (PAR1) acts via a novel Galpha13-dishevelled axis to stabilize beta-catenin levels. J Biol Chem 285:15137–15148
44. Stalheim L, Ding Y, Gullapalli A, Paing MM, Wolfe BL, Morris DR, Trejo J (2005) Multiple independent functions of arrestins in the regulation of protease-activated receptor-2 signaling and trafficking. Mol Pharmacol 67:78–87
45. McCoy KL, Traynelis SF, Hepler JR (2010) PAR1 and PAR2 couple to overlapping and distinct sets of G proteins and linked signaling pathways to differentially regulate cell physiology. Mol Pharmacol 77:1005–1015
46. Lohse MJ (2010) Dimerization in GPCR mobility and signaling. Curr Opin Pharmacol 10:53–58
47. Versteeg HH, Schaffner F, Kerver M, Ellies LG, Andrade-Gordon P, Mueller BM, Ruf W (2008) Protease-activated receptor (PAR) 2, but not PAR1, signaling promotes the development of mammary adenocarcinoma in polyoma middle T mice. Cancer Res 68:7219–7227
48. Schaffner F, Versteeg HH, Schillert A, Yokota N, Petersen LC, Mueller BM, Ruf W (2010) Cooperation of tissue factor cytoplasmic domain and PAR2 signaling in breast cancer development. Blood 116:6106–6113
49. Morris DR, Ding Y, Ricks TK, Gullapalli A, Wolfe BL, Trejo J (2006) Protease-activated receptor-2 is essential for factor VIIa and Xa-induced signaling, migration, and invasion of breast cancer cells. Cancer Res 66:307–314
50. Even-Ram SC, Grisaru-Granovsky S, Pruss D, Maoz M, Salah Z, Yong-Jun Y, Bar-Shavit R (2003) The pattern of expression of protease-activated receptors (PARs) during early trophoblast development. J Pathol 200:47–52
51. O'Brien PJ, Koi H, Parry S, Brass LF, Strauss JF, Wang LP, Tomaszewski JE, Christenson LK (2003) Thrombin receptors and protease-activated receptor-2 in human placentation: receptor activation mediates extravillous trophoblast invasion in vitro. Am J Pathol 163:1245–1254